Role of partial miscibility on pressure buildup due to constant rate injection of CO_2 into closed and open brine aquifers

Simon A. Mathias,[1] Jon G. Gluyas,[1] Gerardo J. González Martínez de Miguel,[1,2] and Seyyed A. Hosseini[3]

Received 15 June 2011; revised 4 November 2011; accepted 8 November 2011; published 17 December 2011.

[1] This work extends an existing analytical solution for pressure buildup because of CO_2 injection in brine aquifers by incorporating effects associated with partial miscibility. These include evaporation of water into the CO_2 rich phase and dissolution of CO_2 into brine and salt precipitation. The resulting equations are closed-form, including the locations of the associated leading and trailing shock fronts. Derivation of the analytical solution involves making a number of simplifying assumptions including: vertical pressure equilibrium, negligible capillary pressure, and constant fluid properties. The analytical solution is compared to results from TOUGH2 and found to accurately approximate the extent of the dry-out zone around the well, the resulting permeability enhancement due to residual brine evaporation, the volumetric saturation of precipitated salt, and the vertically averaged pressure distribution in both space and time for the four scenarios studied. While brine evaporation is found to have a considerable effect on pressure, the effect of CO_2 dissolution is found to be small. The resulting equations remain simple to evaluate in spreadsheet software and represent a significant improvement on current methods for estimating pressure-limited CO_2 storage capacity.

Citation: Mathias, S. A., J. G. Gluyas, G. J. González Martínez de Miguel, and S. A. Hosseini (2011), Role of partial miscibility on pressure buildup due to constant rate injection of CO_2 into closed and open brine aquifers, *Water Resour. Res.*, *47*, W12525, doi:10.1029/2011WR011051.

1. Introduction

[2] A critical design aspect of CO_2 storage systems is that pressure buildup because of CO_2 injection should not exceed the fracture pressure of the overlying caprock [*Mathias et al.*, 2009a, 2009b]. The conventional approach to assessing pressure buildup involves applying a numerical reservoir simulator [*Rutqvist et al.*, 2007, 2008]. Another approach is to numerically integrate the closed-form pressure gradient expression resulting from the *Buckley and Leverett* [1942] (BL) equation [*Saripalli and McGrail*, 2002]. Simplifying assumptions associated with the BL equation include: vertical pressure equilibrium, negligible capillary pressure, incompressible flow, and immiscible displacement. Following an energy minimization approach, *Nordbotten et al.* [2005] derived a similar integral expression, representing a special case of the BL equation where relative permeability is assumed to be a linear function of fluid saturation.

[3] *Mathias et al.* [2009c] applied the method of matched asymptotic expansions to extend Nordbotten's method, to account for moderate fluid and rock compressibility, giving rise to a closed-form pressure buildup equation for CO_2 injection into brine aquifers of infinite lateral extent. Compressibility was assumed large enough that the aquifer has the capacity to retard pressure waves but small enough that fluid density and rock porosity can be assumed constant, the situation generally assumed for most groundwater problems.

[4] More recently, following *Ehlig-Economides and Economides* [2010], *Mathias et al.* [2011] improved their analysis further by invoking a quasi-steady state assumption, allowing the development of a closed-form solution, which takes into account the presence of a far-field impermeable boundary. To properly explore the implications of their simplifying model assumptions, *Mathias et al.* [2011] compared their results with those from the numerical simulator TOUGH2 [*Pruess et al.*, 1999] using the equation of state module, ECO2N [*Pruess*, 2005; *Pruess and Spycher*, 2007]. The assumptions of vertical pressure equilibrium and negligible capillary pressure were found to not significantly affect the pressure buildup estimation. The assumption of constant fluid properties worked well providing an estimate of final pressure that was used to calculate CO_2 fluid properties. The assumption of immiscible flow was also found to be appropriate, providing enough time had passed for the pressure perturbation to reach the outer impermeable boundary of the reservoir. But prior to that, ignoring partial miscibility led to an overestimation of pressure. Permeability reduction due to salt precipitation was ignored.

[5] Miscibility of CO_2 with water leads to CO_2 partially dissolving in brine and water partially vaporizing in the presence of CO_2 [*Spycher et al.*, 2003; *Spycher and Pruess*,

[1]Department of Earth Sciences, Durham University, Durham, UK.
[2]ERC Equipoise Limited, London, UK.
[3]Bureau of Economic Geology, University of Texas Austin, Texas, USA.

0043-1397/11/2011WR011051

2005]. Because of the large interfacial area between the brine and CO_2 that develops at the porescale, it is often assumed that the two phases are in equilibrium with one another. Such a hypothesis gives rise to the CO_2 injection leading to a three-region system [see Figure 2 of *Noh et al.*, 2007]. (1) A dry-out zone develops around the well where all water has been either displaced or vaporized. (2) Surrounding this is a region that contains both a CO_2 rich phase (hereafter referred to as the gas phase) and an aqueous phase. The gas phase contains mostly CO_2 but also contains water at the water in CO_2 solubility limit. The aqueous phase contains mostly brine but also contains CO_2 at the CO_2 in brine solubility limit. (3) Surrounding the two-phase region is another region that contains only brine and is completely free from CO_2.

[6] Although the dry-out zone is free of water, the salt that previously resided in brine remains precipitated in the porespace. Salt precipitation leads to a loss of permeability [*Pruess and Muller*, 2009; *Pruess*, 2009; *Zeidouni et al.*, 2009] and hence a loss in injectivity. But in the numerical study of *Mathias et al.* [2011], accounting for partial miscibility led to an increase in injectivity. This was partially because of the reduction in volumetric flow rate that results from dissolution of CO_2 in brine, but mostly because the dry-out zone had consumed residually trapped brine around the injection well. Residual brine saturations, following CO_2 injection in Canadian sandstones, have been observed as high as 66%, resulting in losses in permeability as high as 90% [*Bennion and Bachu*, 2008]. It can therefore be understood that removal of residual brine by evaporation can potentially lead to significant increases in relative permeability.

[7] *Noh et al.* [2007] and *Pruess* [2009] derived analytical solutions using fractional flow theory [*Orr*, 2007] to look at the effects of partial miscibility on gas saturation distribution assuming no volume change occurs on fluid mixing. *Zeidouni et al.* [2009] improved on these by rigorously satisfying mass continuity and properly accounting for volume change on fluid mixing using methods specified by *Orr* [2007].

[8] Clearly, it would be advantageous to extend the pressure build-up equations of *Mathias et al.* [2009c, 2011] to account for partial miscibility of CO_2 with brine. The pressure buildup equations of *Burton et al.* [2008] and *Ehlig-Economides and Economides* [2010] account for partial miscibility in this way. However, their solutions rely on the specification of a heuristic function to describe relative permeability distribution in space. Furthermore, volume change on fluid mixing is ignored and the location of leading and trailing shock fronts (explained in more detail in section 3) must be specified by a graphical method or an iterative procedure. In this article, the pressure buildup equations of *Mathias et al.* [2009c, 2011] are extended to account for CO_2 brine partial miscibility without the use of heuristic functions. Furthermore, mass balance is rigorously satisfied and closed-form solutions are derived for the locations of the associated shock fronts.

[9] The structure of this article is as follows. The relevant governing equations for two-component two-phase fractional flow are presented. The locations of trailing and leading shock fronts, along with associated changes in volumetric flux, are found by consideration of global mass balance expressions. Linear relatively permeability functions are described and placed in the context of more general power law relative permeability functions. Closed-form solutions for the locations of the shock fronts are obtained. The model is linked with a compressible brine aquifer model and integrated to obtain a closed-form solution for pressure. A comparison of results is made with those obtained using TOUGH2 ECO2N.

2. Two-Component Two-Phase Flow

[10] In section 2, we closely follow the work of *Zeidouni et al.* [2009]. The mass continuity equations for CO_2 and water for one-dimensional, radially symmetric, incompressible, two-phase, two-component radial flow can be written as (adapted from chapter 2 of *Orr*, [2007]),

$$\phi\frac{\partial}{\partial t}(\omega_{ca}\rho_a S_a+\omega_{cg}\rho_g S_g)=-\frac{1}{r}\frac{\partial}{\partial r}[r(\omega_{ca}\rho_a q_a+\omega_{cg}\rho_g q_g)], \quad (1)$$

$$\phi\frac{\partial}{\partial t}(\omega_{wa}\rho_a S_a+\omega_{wg}\rho_g S_g)=-\frac{1}{r}\frac{\partial}{\partial r}[r(\omega_{wa}\rho_a q_a+\omega_{wg}\rho_g q_g)], \quad (2)$$

where ϕ [−] is porosity, t [T] is time, r [L] is radial distance, ω_{ca} [−], ω_{wa} [−], ω_{cg} [−], ω_{wg} [−], are the mass fractions of CO_2 (subscript c) and water (subscript w) in the aqueous (subscript a) and gas (CO_2 rich) (subscript g) phase, respectively, and S_a [−], q_a [LT^{-1}], S_g [−], q_g [LT^{-1}] are the volumetric saturations and fluxes of the aqueous and gas phase, respectively.

[11] Note that here we have assumed radial symmetry. For very large viscosity differences, viscous fingering will occur and the problem will not be radially symmetric as planned [*Zhang et al.*, 1997].

[12] The mass fractions and volumetric saturations are interrelated by $\omega_{ca}+\omega_{wa}+\omega_{sa}=1$, $\omega_{cg}+\omega_{wg}=1$, and $S_a+S_g+S_s=1$ where ω_{sa} [−] is the mass fraction of salt in the aqueous phase and S_s [−] is the volumetric saturation of precipitated salt. Note that although the fluids are assumed incompressible, it is necessary to keep fluid density within the derivatives due to density changes associated with changes in composition.

[13] Introducing the similarity transform

$$z=\frac{\pi\phi\rho_c Hr^2}{M_0 t}, \quad (3)$$

allows the above equations to reduce to [*Orr*, 2007, chapter 4]

$$z=\frac{dH_c}{dG_c}=\frac{dH_w}{dG_w}, \quad (4)$$

where M_0 [MT^{-1}] is a constant mass injection rate of CO_2 of density, ρ_c, [ML^{-3}], H [L] is the thickness of the formation being injected into, and the G and H functions are defined by

$$G_c=c_{ca}S_a+c_{cg}S_g, \qquad H_c=q_D a_c, \quad (5)$$

$$G_w=c_{wa}S_a+c_{wg}S_g, \qquad H_w=q_D a_w, \quad (6)$$

where

$$a_c = c_{ca} f_a + c_{cg} f_g, \qquad a_w = c_{wa} f_a + c_{wg} f_g, \tag{7}$$

and f_a and f_g are the fractional flows of aqueous and gas phase, found from

$$f_a = \frac{q_a}{q_a + q_g}, \qquad f_g = \frac{q_g}{q_a + q_g}, \tag{8}$$

and

$$c_{ca} = \frac{\omega_{ca}\rho_a}{\rho_c}, \qquad c_{wa} = \frac{\omega_{wa}\rho_a}{\rho_c}, \tag{9}$$

$$c_{cg} = \frac{\omega_{cg}\rho_g}{\rho_c}, \qquad c_{wg} = \frac{\omega_{wg}\rho_g}{\rho_c}, \tag{10}$$

$$q_D = \frac{2\pi\rho_c Hr(q_a + q_g)}{M_0}. \tag{11}$$

3. Location of Shocks and Evaluation of q_D

[14] The two-phase two-component system under consideration gives rise to both trailing and leading shocks [*Noh et al.*, 2007; *Zeidouni et al.*, 2009; *Orr*, 2007]. The locations of the leading and trailing shocks, denoted z_L and z_T are the locations (in similarity space), respectively, and can be found from the mass balance equations (similar to *Brinkman* [1949]:

$$H_{c1} - H_{c3} = G_{c1} z_T + \int_{z_T}^{z_L} G_c dz - G_{c3} z_L, \tag{12}$$

$$H_{w1} - H_{w3} = G_{w1} z_T + \int_{z_T}^{z_L} G_w dz - G_{w3} z_L, \tag{13}$$

where $G_{c1} = G_c(z = 0)$, $G_{w1} = G_w(z = 0)$, $H_{c1} = H_c(z = 0)$, and $H_{w1} = H_w(z = 0)$, describe the physical state of the injection fluid and $G_{c3} = G_c(z \to \infty)$, $G_{w3} = G_w(z \to \infty)$, $H_{c3} = H_c(z \to \infty)$, and $H_{w3} = H_w(z \to \infty)$ describe the physical state of the initial reservoir fluid.

[15] Applying the chain rule we have

$$\int_{z_T}^{z_L} G_c dz = \int_{G_{cT}}^{G_{cL}} G_c \frac{dz}{dG_c} dG_c, \tag{14}$$

where $G_{cT} = G_c(z = z_T)$ and $G_{cL} = G_c(z = z_L)$.

[16] The application of integration by parts then leads to

$$\int_{G_{cT}}^{G_{cL}} G_c \frac{dz}{dG_c} dG_c = [G_c z]_{G_{cT}}^{G_{cL}} - \int_{G_{cT}}^{G_{cL}} z dG_c, \tag{15}$$

and substituting equation (4) yields (similar to *Welge* [1952])

$$[G_c z]_{G_{cT}}^{G_{cL}} - \int_{G_{cT}}^{G_{cL}} z dG_c = [G_c z - H_c]_{G_{cT}}^{G_{cL}}, \tag{16}$$

therefore,

$$\int_{z_T}^{z_L} G_c dz = G_{cL} z_L - H_{cL} - G_{cT} z_T + H_{cT}, \tag{17}$$

where $H_{cT} = H_c(z = z_T)$ and $H_{cL} = H_c(z = z_L)$.

[17] Substituting equation (17) into equation (12), yields

$$H_{c1} - H_{c3} = G_{c1} z_T + G_{cL} z_L - H_{cL} - G_{cT} z_T + H_{cT} - G_{c3} z_L. \tag{18}$$

[18] Similarly, from equation (13), we have

$$H_{w1} - H_{w3} = G_{w1} z_T + G_{wL} z_L - H_{wL} - G_{wT} z_T + H_{wT} - G_{w3} z_L, \tag{19}$$

where $G_{wT} = G_w(z = z_T)$, $G_{wL} = G_w(z = z_L)$, $H_{wT} = H_w(z = z_T)$, and $H_{wL} = H_w(z = z_L)$.

[19] To derive an expression for the location of the trailing front, z_T, consider the mass conservation statements for CO_2 and water in the region $0 \le z \le z_T$:

$$H_{c1} - H_{cT} = (G_{c1} - G_{cT}) z_T, \tag{20}$$

$$H_{w1} - H_{wT} = (G_{w1} - G_{wT}) z_T. \tag{21}$$

[20] Rearranging leads to

$$z_T = \frac{H_{c1} - H_{cT}}{G_{c1} - G_{cT}} = \frac{H_{wT} - H_{w1}}{G_{wT} - G_{w1}}, \tag{22}$$

which on substitution back into equations (18) and (19) gives

$$z_L = \frac{H_{cL} - H_{c3}}{G_{cL} - G_{c3}} = \frac{H_{w3} - H_{wL}}{G_{w3} - G_{wL}}. \tag{23}$$

[21] Under such conditions, q_D is piecewise and can be defined by

$$q_D = \begin{cases} q_{D1}, & 0 \le z < z_T \\ q_{D2}, & z_T \le z \le z_L \\ q_{D3}, & z > z_L \end{cases}, \tag{24}$$

and from equations (23) and (22) it can be shown that

$$\frac{q_{D2} a_{cL} - q_{D3} a_{c3}}{G_{cL} - G_{c3}} = \frac{q_{D3} a_{w3} - q_{D2} a_{wL}}{G_{w3} - G_{wL}}, \tag{25}$$

$$\frac{q_{D1} a_{c1} - q_{D2} a_{cT}}{G_{c1} - G_{cT}} = \frac{q_{D2} a_{wT} - q_{D1} a_{w1}}{G_{wT} - G_{w1}}, \tag{26}$$

which, on solving for q_{D2} and q_{D3} lead to [*Orr*, 2007; *Zeidouni et al.*, 2009]

$$q_{D3} = q_{D2} \left[\frac{a_{wL}(G_{cL} - G_{c3}) + a_{cL}(G_{w3} - G_{wL})}{a_{w3}(G_{cL} - G_{c3}) + a_{c3}(G_{w3} - G_{wL})} \right], \tag{27}$$

$$q_{D2} = q_{D1} \left[\frac{a_{w1}(G_{c1} - G_{cT}) + a_{c1}(G_{wT} - G_{w1})}{a_{wT}(G_{c1} - G_{cT}) + a_{cT}(G_{wT} - G_{w1})} \right]. \tag{28}$$

Note that in the dryout-zone ($z < z_T$), volumetric flow rate is unchanged from at the injection point, therefore, $q_{D1} = 1$.

[22] The region where f_g is a differentiable function of S_g is often referred to as the spreading wave [*Orr*, 2007]. Within the spreading wave, from equation (4), it can be shown that [*Orr*, 2007]

$$z = \frac{dH_c}{dG_c} = q_D \frac{df_g}{dS_g}, \tag{29}$$

from which it follows that, providing the shocks are either followed or led by a spreading wave

$$z_L = q_{D2} \frac{df_g}{dS_g}\Big|_{S_g = S_{gL}} \quad \text{and} \quad z_T = q_{D2} \frac{df_g}{dS_g}\Big|_{S_g = S_{gT}}. \tag{30}$$

[23] Substituting these into equations (23) and (22), and considering the definitions provided in equations (5) and (6), gives rise to

$$\frac{df_g}{dS_g}\Big|_{S_g = S_{gs}} = \frac{A_1 + A_2 f_g(S_g = S_{gs})}{A_3 + A_2 S_{gs}}, \tag{31}$$

where

$$\begin{aligned} A_1 &= c_{ca} - (q_{D3}/q_{D2})a_{c3}, & A_2 &= c_{cg} - c_{ca}, \\ A_3 &= c_{ca} - G_{c3}, & S_{gs} &= S_{gL} \end{aligned} \tag{32}$$

$$\begin{aligned} A_1 &= (q_{D3}/q_{D2})a_{w3} - c_{wa}, & A_2 &= c_{wa} - c_{wg}, \\ A_3 &= G_{w3} - c_{wa}, & S_{gs} &= S_{gL} \end{aligned} \tag{33}$$

$$\begin{aligned} A_1 &= (q_{D1}/q_{D2})a_{c1} - c_{ca}, & A_2 &= c_{ca} - c_{cg}, \\ A_3 &= G_{c1} - c_{ca}, & S_{gs} &= S_{gT} \end{aligned} \tag{34}$$

$$\begin{aligned} A_1 &= c_{wa} - (q_{D1}/q_{D2})a_{w1}, & A_2 &= c_{wg} - c_{wa}, \\ A_3 &= c_{wa} - G_{w1}, & S_{gs} &= S_{gT}. \end{aligned} \tag{35}$$

[24] Note that it is necessary to estimate q_{D2} and q_{D3} iteratively except for the special case when the injection composition is free of water (i.e., $a_{w1} = 0$) and the initial reservoir composition is free of CO_2 (i.e., $a_{c3} = 0$).

4. Pure Injection and Reservoir Fluids

[25] Hereafter, it is assumed that the injection fluid is free of water and the reservoir fluid is initially free of CO_2. As a result,

$$G_{c1} = 1 - S_s, \quad a_{c1} = 1, \quad G_{w1} = 0, \quad a_{w1} = 0, \tag{36}$$

$$G_{c3} = 0, \quad a_{c3} = 0, \quad G_{w3} = \omega_{wb}\rho_b/\rho_c, \quad a_{w3} = \omega_{wb}\rho_b/\rho_c \tag{37}$$

where ρ_b [ML^{-3}] and ω_{wb} [−] are the density and water mass fraction, respectively, for brine free of CO_2. Note that $\omega_{wb} + \omega_{sb} = 1$, where ω_{sb} [−] is the salt mass fraction for brine free of CO_2.

[26] Since $a_{w1} = G_{w1} = 0$, S_{gT} can be calculated from equation (35) without knowledge of q_{D2} and q_{D2} can then be calculated from equation (28). Similarly, since $a_{c3} = G_{c3} = 0$, S_{gL} can be calculated from equation (32) without knowledge of q_{D3}, and q_{D3} can then be calculated from equation (27).

[27] The volumetric saturation of precipitated salt, S_s, can be calculated as follows. The mass of brine evaporated is equal to $2\pi\phi H\rho_b(1 - S_{gT})r_T$, where r_T [L] is the radial distance to the trailing shock. The mass of salt precipitated is equal to $2\pi\phi H\omega_{sb}\rho_b(1 - S_{gT})r_T$. The volume of the salt is equal to $2\pi\phi H\omega_{sb}(\rho_b/\rho_s)(1 - S_{gT})r_T$, where ρ_s [ML^{-3}] is the density of precipitated salt. The volume of porespace contained within the trailing shock is equal to $2\pi\phi H r_T$. Therefore, the volumetric saturation of precipitated salt is found from [*Zeidouni et al.*, 2009]

$$S_s = \frac{\omega_{sb}\rho_b(1 - S_{gT})}{\rho_s}. \tag{38}$$

[28] As discussed earlier, when $z_T < z_C$, it is known that $S_{gT} = 1 - S_{ar}$. For most realistic values of S_{ar} it can be assumed $z_T < z_C$.

5. Application of Darcy's Law

[29] Invoking Darcy's Law:

$$q_a = -\frac{kk_{ra}}{\mu_a}\frac{dP}{dr} \tag{39}$$

$$q_g = -\frac{kk_{rg}}{\mu_g}\frac{dP}{dr} \tag{40}$$

where k [L^2] is permeability, P [$ML^{-1}T^{-2}$] is fluid pressure, and k_{ra} [−], μ_a [$ML^{-1}T^{-1}$], k_{rg} [−], and μ_g [$ML^{-1}T^{-1}$] are the relative permeabilities and dynamic viscosities of the aqueous and gas phase, respectively, the fractional flow equation for f_g can be written as,

$$f_g = \left(1 + \frac{\mu_g k_{ra}}{\mu_a k_{rg}}\right)^{-1}. \tag{41}$$

[30] Without much loss of generality, the relative permeability functions can be assumed to take the form of power-laws:

$$k_{ra} = k_{ra0}\left(\frac{1 - S_g - S_{ar}}{1 - S_{gc} - S_{ar}}\right)^m, \tag{42}$$

$$k_{rg} = k_{rg0}\left(\frac{S_g - S_{gc}}{1 - S_{gc} - S_{ar}}\right)^n, \tag{43}$$

where S_{ar} [−] is residual aqueous phase saturation and S_{gc} [−] is critical gas saturation, and k_{ra0} [−], k_{rg0} [−], m [−], and n [−] are end-point relative permeabilities and power law exponents for the aqueous and gas phases, respectively.

[31] The substitution of equations (43) and (42) into equation (41) leads to

$$f_g = \left[1 + \gamma\left(\frac{1 - S_g - S_{ar}}{1 - S_{gc} - S_{ar}}\right)^m \left(\frac{S_g - S_{gc}}{1 - S_{gc} - S_{ar}}\right)^{-n}\right]^{-1}, \tag{44}$$

where

$$\gamma = \frac{\mu_g k_{ra0}}{\mu_a k_{rg0}} \tag{45}$$

and differentiating equation (44) with respect to S_g leads to

$$\frac{df_g}{dS_g} = f_g(1-f_g)\left[\frac{n(1-S_g-S_{ar})+m(S_g-S_{gc})}{(S_g-S_{gc})(1-S_g-S_{ar})}\right]. \tag{46}$$

[32] Interestingly, Figure 1 shows plots of df_g/dS_g (which is linearly proportional to z) against S_g for different values of m and n. For nonlinear relative permeability, S_g is multivalued for given values of df_g/dS_g [*Buckley and Leverett*, 1942]. For the special case when relative permeabilities are linear functions of S_g, S_g is single-valued for given values of df_g/dS_g and there is an inner region, $df_g/dS_g < 0.4$, where $S_g = 1 - S_{ar}$. Furthermore, it can be seen that this special case gradually develops as m and $n \to 1$ (note the two inflection points present for the case when $m = n = 1.1$). See Appendix A for further clarification in this respect.

6. Linear Relative Permeability Functions

[33] It is not possible to obtain closed-form solutions for S_{gT} and S_{gL} by substituting equation (46) into equation (31). However, for the special case when $m = n = 1$ (i.e., when k_{rg} and k_{ra} are linear functions of S_g), equations (44) and (46) reduce to

$$f_g = \left[1 + \gamma\left(\frac{1-S_g-S_{ar}}{S_g-S_{gc}}\right)\right]^{-1} \tag{47}$$

and

$$\frac{df_g}{dS_g} = \frac{\gamma(1-S_{gc}-S_{ar})f_g^2}{(S_g-S_{gc})^2}, \tag{48}$$

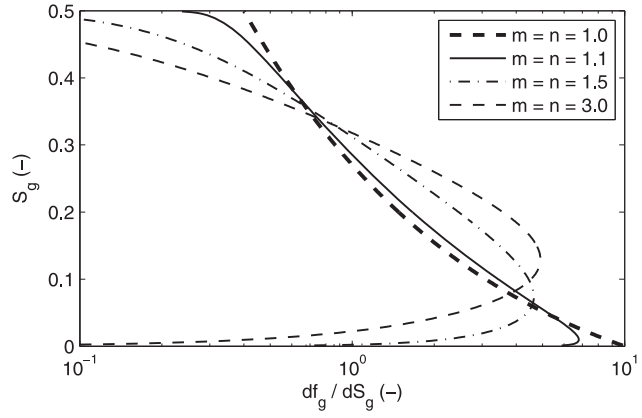

Figure 1. Plots of S_g against df_g/dS_g for different powers according to equation (46) with $\gamma = 0.2$, $S_{gc} = 0$, and $S_{ar} = 0.5$.

which on substitution into equation (31) and solving for S_{gs} leads to

$$S_{gs} = A_4 + \left\{\frac{\gamma(1-S_{gc}-S_{ar})(A_4A_2+A_3)}{(1-\gamma)[(1-\gamma)A_1+A_2]}\right\}^{\frac{1}{2}}, \tag{49}$$

where

$$A_4 = \frac{S_{gc}(A_1+A_2)-\gamma(1-S_{ar})A_1}{(1-\gamma)A_1+A_2} \tag{50}$$

allowing the gas saturations at the leading and trailing shocks to be obtained directly using equations (32) and (35), respectively.

[34] Recalling equation (29) and invoking equations (36) and (37), equation (48) can also be rearranged to get

$$S_g = \begin{cases} 1-S_s, & 0 \le z < z_T \\ 1-S_{ar}, & z_T \le z \le z_C \\ S_{gc} + \dfrac{(1-S_{gc}-S_{ar})}{(1-\gamma)}\left[\left(\dfrac{z_C}{z}\right)^{\frac{1}{2}} - \gamma\right], & z_C < z \le z_L \\ 0, & z > z_L, \end{cases} \tag{51}$$

where

$$z_C = \frac{q_{D2}\gamma}{(1-S_{gc}-S_{ar})}. \tag{52}$$

[35] Note that when $z < z_C$, $S_g = 1 - S_{ar}$. Moreover, when $z_T < z_C$, z_T is no longer located at the beginning of the spreading wave. Consequently, for this special case, equation (31) is invalid for z_T. However, knowing that when $z_T < z_C$, $S_{gT} = 1 - S_{ar}$, and $f_{gT} = 1$, it follows from equation (22) that

$$z_T = \frac{q_{D2}c_{wg}}{c_{wa}S_{ar} + c_{wg}(1-S_{ar})}, \qquad z_T < z_C, \tag{53}$$

where q_{D2} is obtained from equation (28).

7. Solving for Pressure

[36] To obtain an equation for pressure, we return to Darcy's law,

$$q_a + q_g = -k\left(\frac{k_{ra}}{\mu_a} + \frac{k_{rg}}{\mu_g}\right)\frac{dP}{dr}. \tag{54}$$

Applying the similarity transform, z, and the q_D identity (equations (3) and (11)), and then rearranging leads to

$$\frac{dP}{dz} = -\frac{M_0}{4\pi\rho_c Hk}\left(\frac{k_{ra}}{\mu_a} + \frac{k_{rg}}{\mu_g}\right)^{-1}\frac{q_D}{z}. \tag{55}$$

Then given our knowledge of the shock fronts, z_T and z_L,

$$\frac{dP}{dz} = -\frac{M_0}{4\pi\rho_c Hk}\begin{cases}\dfrac{\mu_c q_{D1}}{k_{rs} z}, & 0 \le z < z_T \\ \left(\dfrac{k_{ra}}{\mu_a}+\dfrac{k_{rg}}{\mu_g}\right)^{-1}\dfrac{q_{D2}}{z}, & z_T \le z \le z_L \\ \dfrac{\mu_b q_{D3}}{z}, & z > z_L,\end{cases} \tag{56}$$

where k_{rs} [−] is the permeability reduction factor due to salt precipitation and μ_c [$ML^{-1}\,T^{-1}$] and μ_b [$ML^{-1}\,T^{-1}$] are the dynamic viscosities of water-free CO_2 and CO_2-free brine, respectively.

[37] Integrating with respect to z then yields,

$$P - P_0 = \frac{M_0}{4\pi\rho_c Hk}\begin{cases}\dfrac{\mu_c q_{D1}}{k_{rs}}\ln\left(\dfrac{z_T}{z}\right)+\mu_g q_{D2}F_2(z_T)+\mu_b q_{D3}F_1(z_L), & 0 \le z < z_T \\ \mu_g q_{D2}F_2(z)+\mu_b q_{D3}F_1(z_L), & z_T \le z \le z_L \\ \mu_b q_{D3}F_1(z), & z > z_L,\end{cases} \tag{57}$$

where P_0 [$ML^{-1}\,T^{-2}$] is the initial pressure, $F_1(z) = -\ln z + F_0$ and F_0 is an integration constant yet to be defined, and

$$F_2(z) = -\frac{1}{\mu_g}\int_z^{z_L}\left(\frac{k_{ra}}{\mu_a}+\frac{k_{rg}}{\mu_g}\right)^{-1}\frac{1}{z}dz. \tag{58}$$

[38] Following through the matched asymptotic expansions approach of *Mathias et al.* [2009c, 2011], it can be shown that for a circular closed aquifer of radial extent, r_E [L], (compare with equations (25) and (42) of *Mathias et al.* [2011])

$$F_1(z) = \begin{cases}E_1(\alpha z), & z_E > \dfrac{0.5615}{\alpha} \\ (\alpha z_E)^{-1} - \dfrac{3}{2} + \ln\left(\dfrac{z_E}{z}\right) + \dfrac{z - z_L}{z_E}, & z_E < \dfrac{0.5615}{\alpha},\end{cases} \tag{59}$$

where

$$\alpha = \frac{M_0\mu_b(c_r + c_b)}{4\pi H\rho_c k}, \quad z_E = \frac{\pi\phi\rho_c H r_E^2}{M_0 t}, \tag{60}$$

and E_1 denotes the En function with $n = 1$ (related to the exponential integral function, $\mathrm{Ei}[x]$, via $E_1[x] = -\mathrm{Ei}[-x]$) and c_r [$M^{-1}\,LT^2$] and c_b [$M^{-1}\,LT^2$] are the compressibilities of rock and brine (free of CO_2), respectively.

[39] For an open aquifer of infinite lateral extent, $z_E \to \infty$ and

$$F_1(z) = E_1(\alpha z). \tag{61}$$

Invoking linear relative permeability function, by virtue of equation (51), equation (58) can be evaluated to obtain

$$F_2(z) = \frac{2}{k_{rg0}}\begin{cases}\dfrac{1}{2}\ln\left(\dfrac{z_C}{z}\right)+\dfrac{z_L^{1/2}-z_C^{1/2}}{z_C^{1/2}}, & z \le z_C \\ \dfrac{z_L^{1/2}-z^{1/2}}{z_C^{1/2}}, & z > z_{C.}\end{cases} \tag{62}$$

8. Comparison With TOUGH2 ECO2N

[40] Results from the analytical solution were compared against those from the two-dimensional TOUGH2 simulations previously presented by *Mathias et al.* [2011]. The models assume a fully penetrating well situated at the origin of a two-dimensional radially symmetric flow field of radial extent, r_E. It is also assumed that the relationship between effective brine saturation, S_e [−], and capillary pressure, P_c [$ML^{-1}\,T^{-2}$], is [*van Genuchten*, 1980]

$$S_e = \left(1 + \left|\frac{P_c}{P_{c0}}\right|^{n_v}\right)^{-m_v}, \qquad n_v = \frac{1}{1 - m_v}, \tag{63}$$

and that brine and CO_2 relative permeability are a linear function of S_e. In the absence of residual CO_2 saturation and salt precipitation, effective brine saturation is defined by $S_e = (S_a - S_{ar})/(1 - S_{ar})$. The values of the model parameters used are given in Table 1. Further details are provided by *Mathias et al.* [2011]. The effect of salt precipitation on permeability was ignored.

[41] The analytical solution was evaluated using CO_2 and brine properties from equations of state provided by *Hassanzadeh et al.* [2008]. These incorporate work from a number of authors including *Batzle and Wang* [1992], *Fenghour et al.* [1998], *Spycher et al.* [2003], and *Spycher and Pruess* [2005]. Following *Mathias et al.* [2011], fluid properties were estimated using a preliminary estimate of well pressure (with fluid properties calculated using the initial pressure) that occurs when the pressure disturbance meets the outer boundary of the reservoir (i.e., $z_E = 0.5615/\alpha$). Consequently, a different set of fluid properties was applied to each of the four scenarios studied. These are detailed in Table 2.

Table 1. Parameters Used for the TOUGH2 Simulations

Parameter
Injection rate, $M_0 = 100$ kg s^{-1}
Well radius, $r_W = 0.2$ m
Radial extent, $r_E = 20$ km
Porosity, $\phi = 0.2$
Rock compressibility, $c_r = 4.5 \times 10^{-10}$ Pa^{-1}
Initial pressure, $P_0 = 10$ MPa
Temperature, $T = 40$°C
Mass fraction of salt in brine, $\omega_{sb} = 0.15$
Residual brine saturation, $S_{ar} = 0.5$
Critical gas saturation, $S_{gc} = 0$
End-point relative permeability for CO_2, $k_{rg0} = 0.3$
End-point relative permeability for brine, $k_{ra0} = 1.0$
Permeability reduction factor because of salt precipitation, $k_{rs} = 1$
van Genuchten parameter, $m_v = 0.46$
van Genuchten parameter, $P_{c0} = 19,600$ Pa
Formation thickness, $H = 50$ or 200 m
Permeability, $k = 10^{-13}$ or 10^{-12} m^2

Table 2. Values of Fluid Properties, q_{D2} and q_{D3} for the Four Scenarios Studied

	a	b	c	d
H (m)	50	50	200	200
k (m^2)	10^{-13}	10^{-12}	10^{-13}	10^{-12}
P_{ref} (MPa)	25.13	12.01	14.53	10.58
$\rho_c = \rho_g$ (kg m^{-3})	869	692	746	647
ρ_b (kg m^{-3})	1100	1100	1100	1100
ρ_a (kg m^{-3})	1104	1104	1104	1104
ρ_s (kg m^{-3})	2160	2160	2160	2160
$\mu_c = \mu_g$ (cP)	0.0847	0.0558	0.0630	0.0507
$\mu_b = \mu_a$ (cP)	0.963	0.963	0.963	0.963
c_b (Pa^{-1})	3.54×10^{-10}	3.54×10^{-10}	3.54×10^{-10}	3.54×10^{-10}
ω_{ca} (–)	0.0318	0.0282	0.0289	0.0277
ω_{wg} (–)	0.0021	0.0018	0.0019	0.0016
q_{D2} (–)	1.0003	1.0006	1.0005	1.0006
q_{D3} (–)	0.9821	0.9479	0.9606	0.9355

[42] Figures 1a–1d show the time series of well pressures. The markers are from TOUGH2 simulations and the lines from the analytical solution. The circles and solid lines are output from models that account for partial miscibility of CO_2 and brine. The dashed lines are output from the analytical solution previously presented by *Mathias et al.* [2011], which assumes fully immiscible displacement. Recall that it is the extension of *Mathias et al.* [2011] to account for partially miscible flow, which is the main focus of the current article. Note that well pressures plotted from the two-dimensional radially symmetric TOUGH2 simulation have been vertically averaged.

[43] As discussed in *Mathias et al.* [2011], the distinctive feature between the partially miscible and immiscible simulations is the reduction in pressure rate increase that occurs after 1 hr (1.14×10^{-4} yr). The new analytical solution for partially miscible flow is able to accurately predict this decline in pressure and closely follows the model output from the TOUGH2 simulations.

[44] The cause of the decline is due to the development of the dry-out zone leading to consumption of residual brine and a corresponding increase in CO_2 relative permeability around the well. This can be further understood by studying the saturation and pressure profile plots given in Figure 3. Again, the results plotted from the TOUGH2 simulation have been vertically averaged. The analytical solution is seen to accurately simulate both the extent of the dry-out zone and the saturation of precipitated salt. Similarly, the analytical solution accurately predicts the change in the pressure gradient that occurs in the dry-out zone. Pressures from the immiscible analytical solution of *Mathias et al.* [2011] are shown for comparison.

[45] The effect of CO_2 dissolution into brine manifests itself in two respects. First, in the presence of the leading shock fronts of the saturation profiles (see Figure 3a). Second, in a slight reduction in pressure that occurs at early times (see Figure 2d). The latter effect results from the corresponding reduction in volumetric flow rate, as shown by the q_{D3} values in Table 2. Note that q_{D2} is virtually one, indicating that brine evaporation has little effect on volumetric flow rate.

[46] From a first glance of Figure 2, there is a temptation to dismiss the difference between the partially miscible and miscible simulations, as both simulations converge with large time following the pressure disturbance meeting the outer boundary of the reservoir, which has been arbitrarily set at 20 km from the injection well. However, should the outer boundary be situated further away, equation (59) dictates that pressure will continue to increase along the same linear-log slope, and the miscible and immiscible simulations will continue to diverge. Nevertheless, considering Figure 2c and applying a pressure constraint of 15 MPa, the immiscible model predicts that one can inject for just 8 yr, whereas the miscible model allows injection to continue for up to 22 yr, almost three times as long.

[47] The derivation of the above analytical solution has involved a number of simplifying assumptions including: vertical pressure equilibrium, negligible capillary pressure, and constant fluid properties. However, these three assumptions have been relaxed for the TOUGH2 simulations. As previously discussed by *Mathias et al.* [2011], the constant fluid properties assumption is reasonable providing an estimate of final pressure is used to calculate CO_2 fluid properties. From the comparison of the well pressures in Figure 2, it is clear that both the vertical pressure equilibrium and negligible capillary pressure assumptions are also reasonable for estimating vertically averaged well pressures.

[48] Figure 4 shows profile plots for the case of $k = 10^{-13}$ m^2 and $H = 200$ m. The vertical pressure equilibrium assumption is less realistic for this case, as compared to that presented in Figure 3, due to the larger formation thickness. Rigorous inclusion of gravity in the vertically averaged formulation gives rise to an additional second-order (diffusive like) term in the saturation equation [*Nordbotten and Celia*, 2006; *MacMinn and Juanes*, 2009; *Juanes et al.*, 2010]. Accordingly, there is a notable discrepancy between the vertically averaged gas saturation at 10 yr estimated by the analytical solution and the TOUGH2 simulation. Specifically, gravity segregation has caused the extent of the CO_2 plume to travel further in the TOUGH2 simulation. Nevertheless, as seen in Figures 3 and 4, the analytical solution is able to accurately approximate the radial extent of the dry-out zone, the level of salt precipitation, and the vertically averaged pressure distribution. The reason is that the dry-out zone and the pressures are controlled by the larger velocities situated close around the injection well, which are mostly horizontal due to the horizontal driving force provided by the injection well boundary.

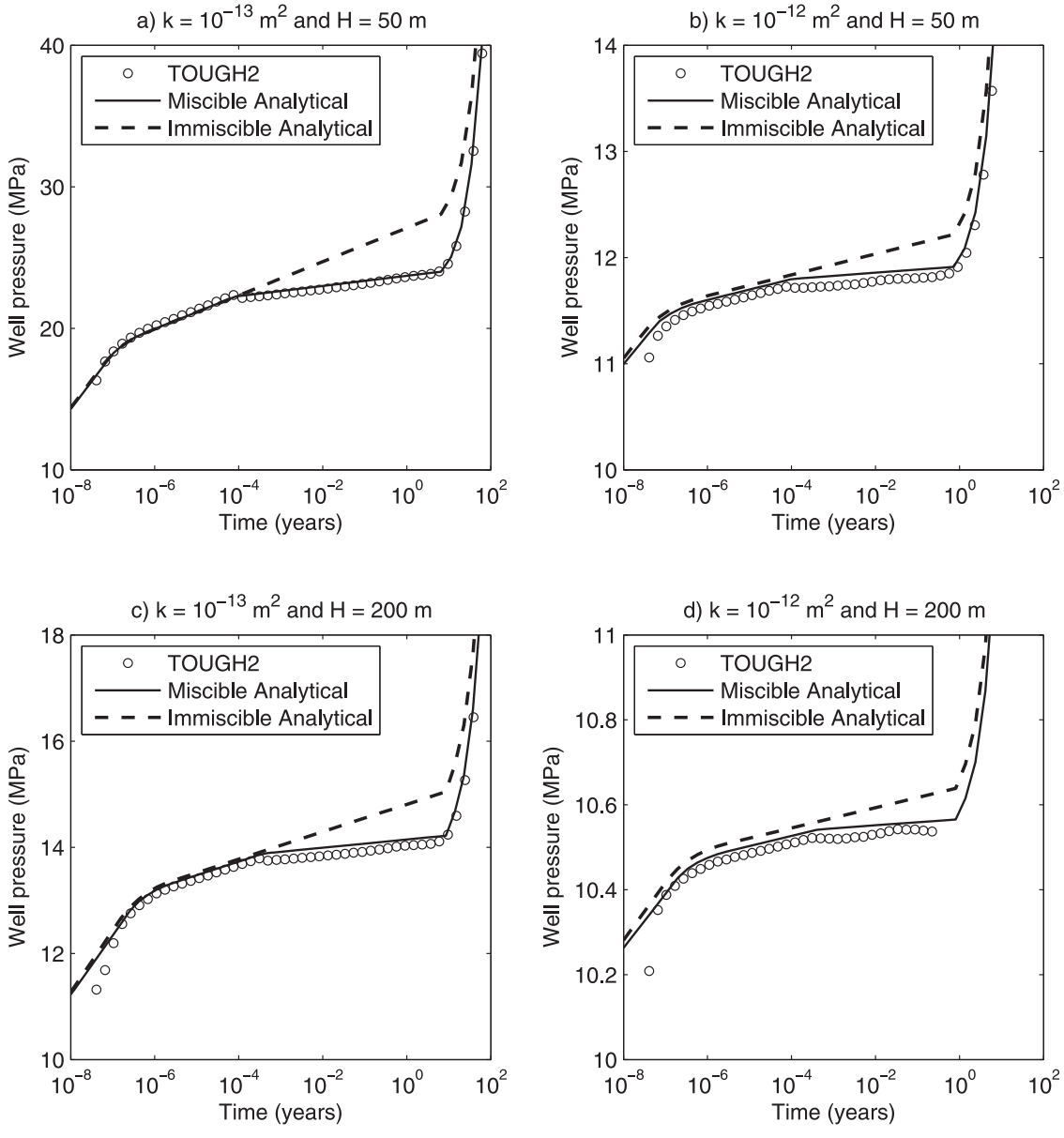

Figure 2. Comparison of well pressures for the four different scenarios (Figures 1a–1d). Results from TOUGH2 have been vertically averaged.

[49] With regard to capillary pressure, according to the simulations studied, there is no significant effect on vertically averaged well pressure (again compare to the results shown in Figure 2). Recall from *Mathias et al.* [2011], the capillary pressure parameters used are the same as previously adopted by *Zhou et al.* [2008]. Of interest is that the dry-out zone can potentially lead to strong capillary forces where CO_2 will tend to reimbibe toward the well, increasing the amount of salt precipitated in the dry-out zone. Accounting for counter-current imbibition is found to be particularly important when seeking to estimate the quantity of CO_2 that becomes residually trapped after injection has ceased [*Javaheri and Jessen*, 2011]. But comparing results from models which ignored and included capillary pressure (and in turn, counter-current imbibition), *Pruess and Muller* [2009] found that inclusion of capillary pressure effects is unlikely to increase salt precipitation by more than a factor of order 1.1. Furthermore, notable changes in the shape of the dry-out zone, as a result of counter-current imbibition, were only observed for the exceptionally small injection rate of 0.25 kg s^{-1} (see Figure 7 in the work of *Pruess and Muller* [2009]). Injection rates of practical interest for commercial scale projects typically range from 3 to 120 kg s^{-1} [*Oldenburg et al.*, 2004; *Zhou et al.*, 2008]. In the current study, an injection rate of 100 kg s^{-1} is assumed.

9. Summary and Conclusions

[50] The objective of this study was to extend the pressure buildup equations of *Mathias et al.* [2009c, 2011] to account for effects associated with the partial miscibility of CO_2 and brine. These include evaporation of water into the CO_2 rich phase, dissolution of CO_2 into brine, and salt precipitation. This was achieved by applying two-component

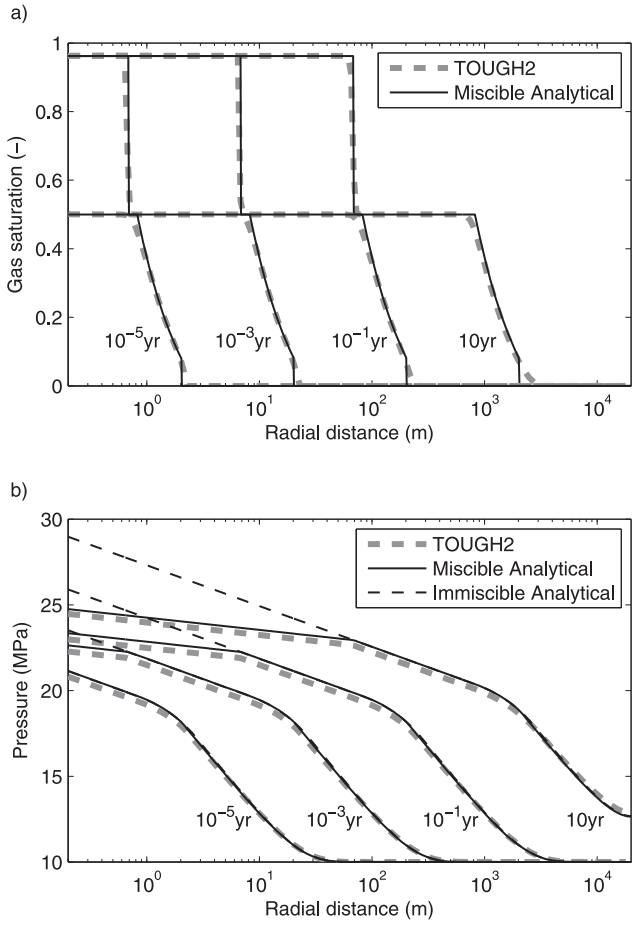

Figure 3. Comparison of (a) gas saturation and (b) pressure distributions for the scenario shown in Figure 2a, i.e., $k = 10^{-13}$ m^2 and $H = 50$ m. Results from TOUGH2 have been vertically averaged.

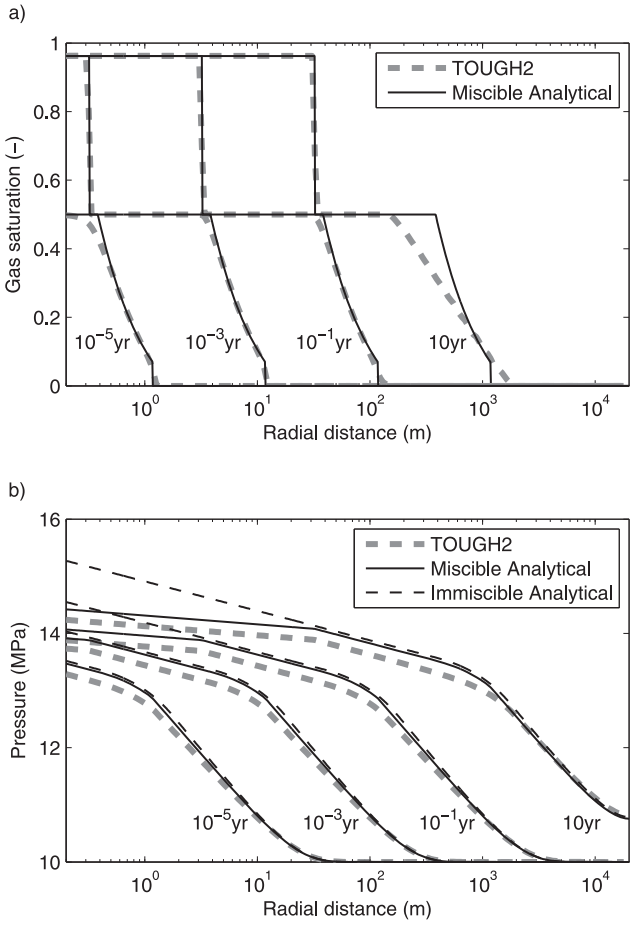

Figure 4. Comparison of (a) gas saturation and (b) pressure distributions for the scenario shown in Figure 2c, i.e., $k = 10^{-13}$ m^2 and $H = 200$ m. Results from TOUGH2 have been vertically averaged.

two-phase fractional flow theory [*Orr*, 2007] in conjunction with linear relative permeability functions, to derive a gas saturation distribution function (equation (51)). From this, the relative permeability distribution was obtained and integrated to obtain the new pressure buildup equation, equation (57). In general (i.e., for arbitrary relative permeability functions), the evaluation of equaion (57) requires the numerical integration of equation (58). But for the special situation when relative permeability is a linear function of saturation, equation (58) integrates exactly to yield the closed-form expression given in equation (62).

[51] Similar equations have previously been presented by *Burton et al.* [2008]. However, the difference here is that we additionally account for volume change on mixing and provide closed-form expressions for the location of the shock fronts for the special case when relative permeability is a linear function of saturation (obtained using either equations (30), (48), and (49) or equation (53)). Furthermore, the pressure equations can be used to describe both closed and open aquifers (using either equations (59) or (61)).

[52] The analytical solution was tested by comparison against output from TOUGH2 ECO2N, previously presented by *Mathias et al.* [2009c]. Results from the analytical solution were obtained using fluid properties provided by equations of state documented by *Hassanzadeh et al.* [2008]. The analytical solution was compared to results from TOUGH2 and found to accurately approximate the extent of the dry-out zone around the well, the resulting permeability enhancement due to residual brine evaporation, the volumetric saturation of precipitated salt, and the vertically averaged pressure distribution in both space and time for the four scenarios studied.

[53] While the effect of brine evaporation can be considerable, the effect of CO_2 dissolution is small. CO_2 dissolution into brine leads to a modest reduction in volumetric flow rate beyond the two-phase region, resulting in a reduction in pressure that occurs throughout injection. For the scenarios studied, volumetric flow rate reduction was found to be less than 7% and the effect on pressure was barely noticeable.

[54] The resulting equations remain simple to evaluate in spreadsheet software, and can be easily implemented in currently available storage capacity estimation frameworks [e.g., *Mathias et al.*, 2009a].

Appendix A: Shock Construction With Linear Relative Permeability

[55] Figure 1 illustrates an unusual feature of the linear relative permeability function, namely that the inflection points in the S_g versus df_g/dS_g function are lost. Linear

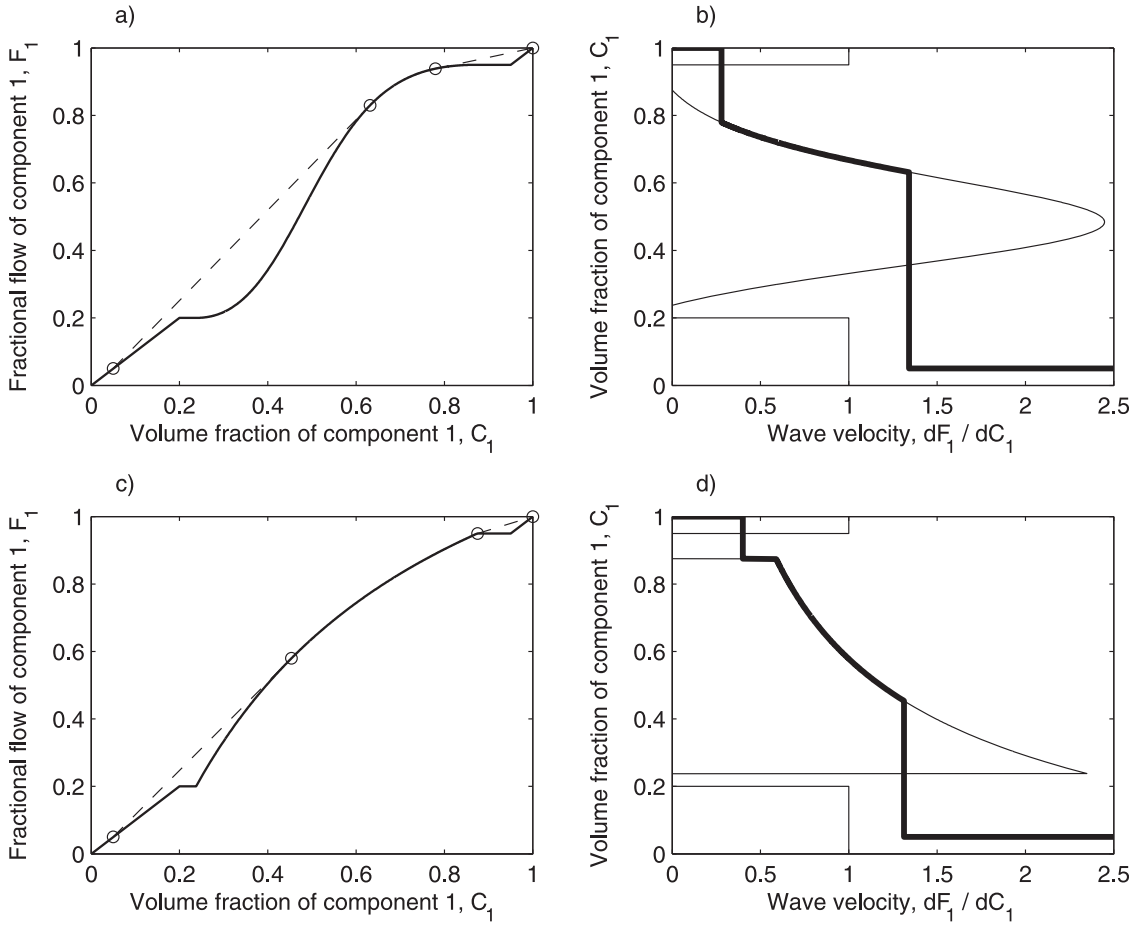

Figure 5. Plots explaining the leading and trailing shock constructions for the example presented by *Orr* [2007, be sure this isn't linked to Figure 4 of this article]. Figures 5a and 5b show results assuming quadratic relative permeability. Figures 5c and 5d show results assuming linear relative permeability. The location of the shocks are found from the gradients of the dashed lines in 5a and 5c. (b, d) Complete fractional flow functions and final solutions with shocks in place are plotted as thinner and thicker lines, respectively.

relative permeability therefore leads to situations where the trailing shock is not located at the beginning of the spreading wave (recall equation (53)). This point is demonstrated further in Figure 5, which compares the example previously presented by *Orr* [2007, his Figure 4.9], assuming quadratic relative permeability (i.e., with equations (42) and (43) and $m = n = 2$), with an identical example assuming linear relative permeability (i.e., $m = n = 1$).

References

Batzle, M., and Z. Wang (1992), Seismic properties of pore fluids, *Geophysics*, *57*, 1396–1408.

Bennion D. B., and S. Bachu (2008), Drainage and imbibition relative permeability relationships for supercritical CO_2/brine and H_2S/brine systems in intergranular sandstone, carbonate, shale, and annhydrite rocks, *SPE Reservoir Eval. Eng.*, *11*, 487–496.

Brinkman, H. C. (1949), Calculations on the flow of heterogenous mixtures through porous media, *App. Sci. Res.*, *A1*, 333–346.

Buckley, S. E., and M. C. Leverett (1942), Mechanism of fluid displacement in sands, *Trans. AIME*, *146*, 187-196.

Burton, M., N. Kumar, and S. L. Bryant (2008), Time-dependent injectivity during CO_2 storage in aquifers, 15 pp., *SPE/DOE Improved Oil Recovery Symposium Tulsa*, SPE 113937, doi:10.2118/113937-MS.

Ehlig-Economides, C. A., and M. J. Economides (2010) Sequestering carbon dioxide in a closed underground volume, *J. Pet. Sci. Eng.*, *70*, 123–130, doi:10.1016/j.petrol.2009.11.002.

Fenghour, A., W. A. Wakeham, and V. Vesovic (1998), The viscosity of carbon dioxide, *J. Phys. Chem. Ref. Data*, *27*, 31–44.

Hassanzadeh, H., M. Pooladi-Darvish, A. M. Elsharkawy, D. W. Keith, and Y. Leonenko (2008), Predicting PVT data for CO_2-brine mixtures for black-oil simulation of CO_2 geological storage, *Int. J. Greenhouse Gas Control*, *2*, 65–77.

Javaheri, M., and K. Jessen (2011), Integration of counter-current relative permeability in the simulation of CO_2 injection into saline aquifers, *Int. J. Greenhouse Gas Control*, *5*, 1272–1283, doi:10.1016/j.ijggc.2011.05.015.

Juanes, R., C. W. MacMinn, and W. L. Szulczewski (2010), The footprint of the CO_2 plume during carbon dioxide storage in saline aquifers: Storage efficiency for capillary trapping at the basin scale, *Transp. Porous Med.*, *82*, 19–30, doi:10.1007/s11242-009-9420-3.

MacMinn, C. W., and R. Juanes (2009), Post-injection spreading and trapping of CO_2 in saline aquifers: impact of the plume shape at the end of injection, *Comput. Geosci.*, *13*, 483–491, doi:10.1007/s10596-009-9147-9.

Mathias, S. A., P. E. Hardisty, M. R. Trudell, and R. W. Zimmerman (2009a), Screening and selection of sites for CO_2 sequestration based on pressure buildup, *Int. J. Greenhouse Gas Control*, *3*, 577–585, doi:10.1016/j.ijggc.2009.05.002.

Mathias, S. A., P. E. Hardisty, M. R. Trudell, and R. W. Zimmerman (2009b), Erratum to Screening and selection of sites for CO_2 sequestration

based on pressure buildup, *Int. J. Greenhouse Gas Control*, *4*, 108–109, doi:10.1016/j.ijggc.2009.11.004.

Mathias, S. A., P. E. Hardisty, M. R. Trudell, and R. W. Zimmerman (2009c), Approximate solutions for pressure buildup during CO_2 injection in brine aquifers, *Transp. Porous Media*, *79*, 265–284, doi:10.1007/s11242-008-9316-7.

Mathias, S. A., G. J. González Martínez de Miguel, K. E. Thatcher, and R. W. Zimmerman (2011), Pressure buildup during CO_2 injection into a closed brine aquifer, *Transp. Porous Media*, *89*, 383–397, doi:10.1007/s11242-011-9776-z.

Noh, M., L. W. Lake, S. L. Bryant, and A. Araque-Martinez (2007), Implications of coupling fractional flow and geochemistry for CO_2 injection in aquifers, *SPE Reservoir Eval. Eng.*, *10*, 406–414.

Nordbotten, J. M., and M. A. Celia (2006), Similarity solutions for fluid injection into confined aquifers, *J. Fluid Mech.*, *561*, 307–327, doi:10.1017/S0022112006000802.

Nordbotten, J. M., M. A. Celia, and S. Bachu (2005), Injection and storage of CO_2 in deep saline aquifers: Analytic solution for CO_2 plume evolution during injection, *Transp. Porous Media*, *58*, 339–360, doi:10.1007/s11242-004-0670-9.

Oldenburg, C. M., S. J. Stevens, and S. M. Benson (2004), Economic feasibility of carbon sequestration with enhanced gas recovery (CSEGR), *Energy*, *29*, 1413–1422, doi:10.1016/j.energy.2004.03.075.

Orr, F. M., Jr. (2007), *Theory of Gas Injection Processes*, 381 pp., Tie-Line Publications, Copenhagen, Denmark.

Pruess, K. (2005), ECO2N: A TOUGH2 fluid property module for mixtures of water, NaCl, and CO_2, *Rep. LBNL-57952*, Lawrence Berkeley National Laboratory, Berkeley, Calif.

Pruess, K. (2009), Formation dry-out from CO_2 injection into saline aquifers: 2. Analytical model for salt precipitation, *Water Resour. Res.*, *45*, W03403, doi:10.1029/2008WR007102.

Pruess, K., and N. Muller (2009), Formation dry-out from CO_2 injection into saline aquifers: 1. Effects of solids precipitation and their mitigation, *Water Resour. Res.*, *45*, W03402, doi:10.1029/2008WR007101.

Pruess, K., and N. Spycher (2007), ECO2N: A fluid property module for the TOUGH2 code for studies of CO_2 storage in saline aquifers, *Energy Convers. Manage.*, *48*, 1761–1767, doi:10.1016/j.enconman.2007.01.016.

Pruess, K., C. M. Oldenburg, and G. Moridis (1999), TOUGH2 users guide, version 2.0., *Rep. LBNL-43134*, Lawrence Berkeley National Laboratory, Berkeley, Calif.

Rutqvist, J., J. T. Birkholzer, F. Cappa, and C. F. Tsang (2007), Estimating maximum sustainable injection pressure during geological sequestration of CO_2 using coupled fluid flow and geomechanical fault-slip analysis, *Energy Convers. Manag.*, *48*, 1798–1807.

Rutqvist, J., J. T. Birkholzer, and C. F. Tsang (2008), Coupled reservoir-geomechanical analysis of the potential for tensile and shear failure associated with CO_2 injection in multilayered reservoircaprock systems, *Int. J. Rock. Mech. Min. Sci.*, *45*, 132–143.

Saripalli P., and P. McGrail (2002), Semi-analytical approaches to modeling deep well injection of CO_2 for geological sequestration, *Energy Conv. Manag.*, *43*, 185–198.

Spycher, N., and K. Pruess (2005), CO_2–H_2O mixtures in the geological sequestration of CO_2. II. Partitioning in chloride brines at 12100°C and up to 600 bar, *Geochim. Cosmochim. Acta*, *69*, 3309–3320, doi:10.1016/j.gca.2005.01.015.

Spycher, N., K. Pruess, and J. Ennis–King (2003), CO_2–H_2O mixtures in the geological sequestration of CO_2. I. Assessment and Calculation of Mutual Solubilities from 12 to 100°C and up to 600 bar, *Geochim. Cosmochim. Acta*, *67*, 3015–3031, doi:10.1016/S0016-7037(03)00273-4.

van Genuchten, M. T. (1980), A closed form equation for predicting the hydraulic conductivity of unsaturated soils, *Soil. Sci. Soc. Am. J.*, *44*, 892–898.

Welge, H. J. (1952), A simplified method for computing oil recovery by gas or water drive, *Trans. AIME*, *195*, 91–98.

Zeidouni, M., M. Pooladi-Darvish, and D. Keith (2009), Analytical solution to evaluate salt precipitation during CO_2 injection in saline aquifers, *Int. J. Greenhouse Gas Control*, *3*, 600–611, doi:10.1016/j.ijggc.2009.04.004.

Zhang, H. R., K. S. Sorbie, and N. B. Tsibuklis (1997), Viscous fingering in five-spot experimental porous media: New experimental results and numerical simulation, *Chem. Eng. Sci.*, *52*, 37–54, doi:10.1016/S0009-2509(96)00382-X.

Zhou, Q., J. Birkholzer, C. Tsang, and J. Rutqvist (2008), A method for quick assessment of CO_2 storage capacity in closed and semi-closed saline formations, *Int. J. Greenhouse Gas Control*, *2*, 626–639, doi:10.1016/j.ijggc.2008.02.004.

J. G. Gluyas and S. A. Mathias, Department of Earth Sciences, Durham University, Durham DH1 3LE, UK. (s.a.mathias@durham.uk)

G. J. González Martínez de Miguel, ERC Equipoise Limited, 28 Tanfield Rd., London CR0 1BT, UK.

S. A. Hosseini, Bureau of Economic Geology, University of Texas Austin, University Station, Austin, Texas 78713-8924, USA.